Journal of Alloys and Compounds 774 (2019) 565–572

Contents lists available at ScienceDirect

Journal of Alloys and Compounds

journal homepage: http://www.elsevier.com/locate/jalcom

Copper and carbon co-encapsulated tin dioxide nanocrystals for high performance lithium ion batteries

Tao Li, Bing Liu[*], Huanqing Liu, Jiajia Zou, Yanhua Ding, Tuo Xin, Yiqian Wang[**]

College of Physics and Cultivation Base for State Key Laboratory, Qingdao University, No. 308 Ningxia Road, Qingdao, 266071, People's Republic of China

ARTICLE INFO

Article history:
Received 23 April 2018
Received in revised form
22 August 2018
Accepted 24 August 2018
Available online 27 August 2018

Keywords:
Lithium ion battery
SnO_2 composites
Co-encapsulated
High conductivity
Electrochemical performance

ABSTRACT

Copper and carbon co-encapsulated tin dioxide nanocrystals with a diameter of about 8–10 nm are synthesized through a simple solution system and following calcination in N_2 atmospheres. Ascorbic acid acts as a reducing agent to facilitate rapid precipitation of polycrystalline and control the microscopic morphology of the products. The ultra-small SnO_2 grains with co-encapsulated copper and carbon shells can effectively increase the stability of the active materials. The copper and carbon coatings also help to increase the conductivity of the electrode materials. When used as anode materials of lithium-ion batteries, the composite exhibits good electrochemical performance with a high specific capacity of 670.3 mAh g^{-1} after 50 cycles at a current density of 0.2 A g^{-1}. When the current density reaches 0.4 A g^{-1}, the reversible capacity is approximately 452 mAh g^{-1} after 200 cycles. The results show that the composite material with high conductivity is a good choice for lithium ion battery anode materials.

1. Introduction

Rechargeable batteries with high energy density, long life, small size, light weight, safety, environmental compatibility and low cost have been developed to power a wide variety of applications, such as for portable consumer electronic devices, hybrid electric vehicles (HEV), electric vehicles (EV) and large-scale electricity storage in smart grids [1–3]. The ever-growing market demand for batteries allows researchers to continuously improve the properties and electrochemical stability. The performance of the battery depends mainly on the electrochemical properties of the electrode materials, so the future of electrochemical storage will depend on the design of the new structure and improvement of the material phase composition [4,5]. For lithium ion batteries (LIBs), graphite-based anode materials are still in use since the first commercial lithium-ion battery launched by Sony in 1991. Yet, the specific capacity of the modified graphite or the graphite-based anode material is only 372 $mAh \cdot g^{-1}$. The low theoretical capacity of graphite limits the further development and application of LIBs. Therefore, with the characteristics of high specific capacities (usually multiple times higher than graphite-based materials) and large-scale manufacturing, metal oxides have always been potential electrode materials for LIBs and supercapacitors [6]. However, metal oxides generally suffer from poor ion transport kinetics and volume expansion during charging/discharging processes. So, it is necessary to design new nanostructures and hybrid electrode materials to improve the electrical conductivity and structural stability of the electrode materials.

Due to high theoretical capacity (782 $mAh \cdot g^{-1}$ 4.4 equivalent of lithium per SnO_2, and 1494 $mAh \cdot g^{-1}$ 8.4 equivalent of lithium per SnO_2) [7], tin dioxide is considered as a promising anode material for LIBs [8]. In a Li/SnO_2 half-cell, the electrochemical processes can be summarized by the following formulas:

$$SnO_2 + 4Li + 4e^- \rightarrow Sn + 2Li_2O \tag{1}$$

$$Sn + xLi^+ + xe^- \leftrightarrow Li_xSn \ (0 \le x \le 4.4) \tag{2}$$

Like other metal oxides, the volume expansion of SnO_2 electrodes is typically about 200% upon lithium insertion, resulting in the rapid fading of capacity [9]. Many strategies have been developed to solve this problem, including designing various structures and synthesizing different chemical components. The research based on electrode is as follows: 1) 0D quantum dots [10], 2) 1D nanorods, nanowires, nanotubes, nanofibers [11], 3) 2D nanosheets, nanofilms [12], 4) 3D nanospheres, hollow structures [13], 5) Carbon coating [14], 6) Preparation of graphene/SnO_2 composites [15].

---

[*] Corresponding author.
[**] Corresponding author.
E-mail addresses: bing_liu@qdu.edu.cn (B. Liu), yqwang@qdu.edu.cn (Y. Wang).

https://doi.org/10.1016/j.jallcom.2018.08.237
0925-8388/

Lou's group [8] and the Rogach group [16] have studied in detail the synthesis of SnO_2-based nanomaterials with various structures and chemical compositions, and their application as anode electrodes for LIBs. The morphological improvement and design will help to effectively relieve the volume expansion of the material during charge and discharge. But all of these factors are more difficult to increase the ion transport kinetics.

Conductivity has always been one of important factors affecting the performance of electrode materials in LIBs. Increasing the electronic conductivity and ion diffusion rate of anode and cathode materials is an effective way to improve the capacity of lithium ion batteries [17]. Copper (Cu) has high conductivity and high strength [18]. Metallic Cu, which does not react with the electrolyte and lithium ions during the electrochemical process, is employed to serve as the supporting layer because it has high stability and ideal conductivity [19]. Therefore, doping Cu in electrode materials is a feasible path to improve the conductivity of lithium ion batteries and improve its performance. Several researches are concerned about the Cu/SnO_2 electrode and have shown improved cycling performance in Li-ion and Li-S batteries [20]. In this work, we designed and synthesized copper and carbon co-encapsulated tin dioxide ($C@Cu@SnO_2$) nanocrystals through a simple solution system and following carbonization in N_2 atmospheres. When used as anode electrode materials, they exhibited good lithium storage performance with a capacity of 666.8 mAh g^{-1} after 50 cycles at a density current of 0.2 A g^{-1}. Even when recycled at high density current up to 2 A g^{-1}, they can still provide more than 450 mAh g^{-1} capacity. The good electrochemical performance benefits from the composite electrode material. The carbon and copper shells in the composite materials act as a buffer layer, efficiently reducing the volume change, and the existence of Cu effectively reduces the electrical resistance and improves the conductivity.

2. Experimental section

2.1. Materials synthesis

All chemicals used were of analytical grade without further purification. The copper and carbon co-encapsulated tin dioxide nanocrystals were synthesized by a simple hydrothermal process and following carbonization in N_2 atmospheres. In a typical procedure, 2 mmol sodium stannate trihydrate ($Na_2SnO_3 \cdot 3H_2O$) and 2 mmol ascorbic acid were added to 30 mL distilled water under stirring at room temperature for 20 min; similarly, different amounts of copper chloride (2%, 5%, 10%, 20% according to $Na_2SnO_3 \cdot 3H_2O$) and ascorbic acid were added to 30 mL of distilled water with stirring. And then the $CuCl_2$-Vc solution was added to the Na_2SnO_3-Vc solution. After stirring for 60 min, the solution was transferred to a 80 mL Teflon-lined stainless steel autoclave and maintained at 180 °C for 12 h to produce a brown precipitate. After being naturally cooled to room temperature, the obtained brown precipitation was collected by centrifugation and washed several times with distilled water and ethanol, and dried in air at room temperature. The carbonization of the products was annealed in N_2 stream at 500 °C for 2 h at a ramp rate of 5 °C min^{-1}. Based on the experimental data in the latter part of this article, the products synthesized by 20% $CuCl_2$ were studied and analyzed.

2.2. Materials characterization

The crystal structure and phase purity of the products were characterized by X-ray power diffraction (Bruker, D8 Advance X-ray diffractometer, $Cu_{K\alpha}$ ($\lambda = 1.5406$ Å). XRD patterns were recorded from 20° to 80° (2θ) with a scanning step of $1° \cdot min^{-1}$ at 40 kV voltages and 40 mA current. The structural refinement of the obtained phases and profile analysis of the related diffraction patterns were carried out with the program TOPAS (general profile and structure analysis for powder diffraction data, Bruker Analytical X-ray Systems) [21–24]. The micro-structure and morphology were investigated by field-emission scanning electron microscope (JEOLS-4800) and transmission electron microscope (JEM-2010). The surface area and pore size of the products were measured using a Belsorp-max surface area detecting instrument by N_2 physisorption at 77 K. Raman spectra was recorded using a RM 2000 Microscopic Confocal Raman Spectrometer (Renishaw PLC, England) with an Ar laser at a wavelength of 514.5 nm. XPS were recorded using ESCALAB 250 spectrometer (Perkin-Elmer) to characterize the surface composition.

2.3. Electrochemical measurements

To test the electrochemical performance of the products, two-electrode CR2025 coin cell with working electrode and lithium foil as the counter electrode were assembled in an argon-filled glove-box. The working electrodes were prepared by coating slurry onto a Cu foil substrate. The slurry was made by the active materials, conductive carbon black, and polyvinylidene (PVDF) in the weight ratio of 70:15:15 dispersed in N-methyl pyrrolidone (NMP). After coating, the electrodes were pressed at 10 MPa and dried at 120 °C under vacuum for 24 h. A solution of 1M $LiPF_6$ in ethylene carbonate (EC)/dimethyl carbonate (DMC)/diethyl carbonate (DEC) (1:1:1 in volume) was used as the electrolyte. Galvanostatic cycling performances of the homemade coin cells were measured on a multichannel battery testing system (LAND CT2001A) with cutoff voltage of 3.0–0.01 V versus Li/Li^+. CV curves were recorded on a CHI-660D potentiostat at a scanning rate of 0.5 mV s^{-1}. The impendence spectra were obtained by applying a sine wave with amplitude of 5 mV over the frequency range from 100 kHz to 0.01 Hz.

3. Results and discussion

The X-ray power diffraction (XRD) patterns were employed to characterize the crystal structure of the copper and carbon co-encapsulated tin dioxide nanocrystals. Fig. 1a shows the XRD patterns of the as-prepared products (20% $CuCl_2$) obtained from the hydrothermal treatment and the XRD patterns of the products after calcination in N_2 at 500 °C for 2 h, respectively. From Fig. 1a, we can infer that the peaks (*) centered at 26.5, 33.9, 51.8, 65.9° can be indexed to the (110), (101), (211) and (112) planes assigned to SnO_2, which was consistent with the tetragonal rutile SnO_2 phase (JCPDS card NO. 41-1445, SG: $P4_2/mnm$, $a_0 = 4.74$ Å, and $c_0 = 3.18$ Å) [25]. And the peak (#) at 43.2 and 50.2° are consistent with copper. It can be observed that the peak intensity of SnO_2 relative to bulk materials is low and wide, indicating the small crystal size of the SnO_2 nanocrystals. After calcination in N_2, the diffraction peaks of the products narrowed and peak intensity increased. The phase composition of SnO_2 and Cu did not change significantly. No other impurity peaks were detected, indicating the purity of the $Cu@C@SnO_2$ composites. (XRD-1).

Fig. 1(b–e) shows field-emission scanning electron microscopy (FE-SEM) images of the samples before (1b and c) and after (1d and e) calcination. It can be clearly seen that the sample before calcination consists of very small spherical particles, and each particle is assembled from numerous primary nanocrystals, creating enough space and holes, which facilitates Li^+ transfer during charge and discharge process. Ascorbic acid acts as a reducing agent to facilitate rapid precipitation of polycrystalline and control the microscopic morphology of the products. After calcination, the particles become larger and the crystallization is enhanced. The

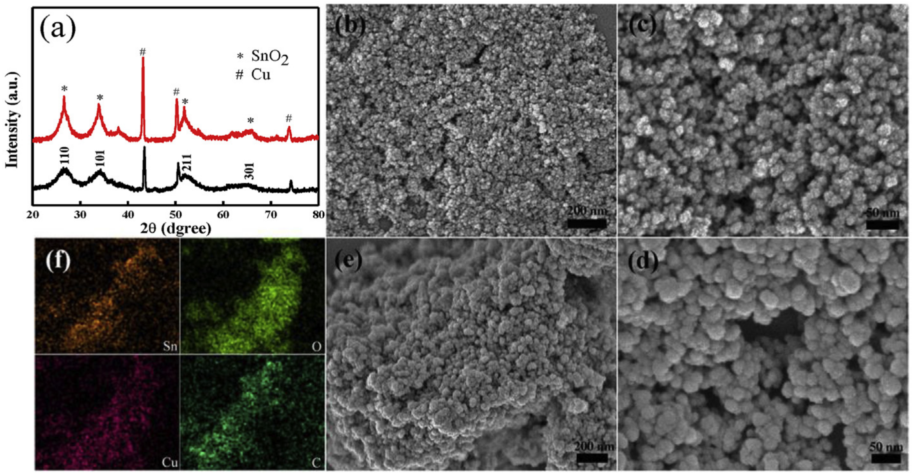

Fig. 1. (a) XRD patterns of the C@Cu@SnO_2 products; (b) Field-FE-SEM images before (b, c) and after (d, e) calcination of the samples; (f) Element mapping analysis of the annealed C@Cu@SnO_2 products.

corresponding element mapping analysis (Fig. 1f) of the annealed sample confirms that the Sn, Cu and O elements ae uniformly distributed in the samples.

To obtain the crystal information and the composition of the complex, XRD diffraction patterns were analyzed using the TOPAS program. Different amounts of $CuCl_2$ (2%, 5%, 10%, 20% according to $Na_2SnO_3 \cdot 3H_2O$) were used as raw material to control the copper content. As shown in Fig. 2, the amount of the loaded Cu on SnO_2 varies with the dosage, and the crystal diffraction peaks show that the Cu content is 1.87%, 2.24%, 3.46% and 6.82% for different dosage of $CuCl_2$ (2%, 5%, 10% and 20%, respectively). An increase in Cu content significantly increases the conductivity. However, the presence of a large amount of Cu also reduces the overall energy density of the battery. Therefore, we choose 6.82% of Cu as the test sample instead of trying a larger dose of $CuCl_2$.

The composition of the C@Cu@SnO_2 sample can be further determined by X-ray photoelectron spectroscopy (XPS). Apart from a weak C 1s peak at 284.4 eV and Cu 2*p* peak at about 932 and 952 eV, only Sn and O related core peaks can be detected in the survey XPS spectrum (Fig. 3a). It involves six distinct peaks of 26.6 (Sn 4d), 486.2 (Sn $3d_{5/2}$), 494.6 (Sn $3d_{3/2}$), 715.5 (Sn 3*p*), 758.2 (Sn 3*p*) and 530.2 eV (O 1s), which are the characteristic of tin dioxides [20,25]. In Fig. 3b, two strong peaks centered at 486.2 and 494.6 eV are attributed to Sn $3d_{5/2}$ and Sn $3d_{3/2}$ states, respectively. The Sn 3d spectra are in good agreement with the characteristic bands of SnO_2, indicating that tin is a Sn (IV) state.

The morphology and microstructure of the copper and carbon co-encapsulated tin dioxide (C@Cu@SnO_2) nanocrystals are further investigated by transmission electron microscopy (TEM). Fig. 4a and b shows low and high magnification TEM images of the annealed C@Cu@SnO_2 sample, respectively. Fig. 4a clearly shows that the sample consists entirely of relatively uniform spheres, and Fig. 4b shows that the size of the crystals is less than 10 nm in diameter, which is also confirmed by SEM observation. Moreover, an amorphous carbon layer with a thickness about 2 nm can also be clearly observed at the edge of the spheres. Additionally, as disclosed in the HRTEM image (Fig. 4c), the lattice spacing is approximately 0.335 nm, which corresponds to the (110) plane of monoclinic SnO_2 phase. The selected area electron diffraction (SAED) (Fig. 4d) pattern shows a single spot associated with concentric rings, indicating the polycrystalline nature of the C@Cu@SnO_2 spheres. And the ascorbic acid in the system acts as a reducing agent to facilitate rapid precipitation of polycrystalline and control the microscopic morphology of the products.

In order to determine the sphere diameter and crystallite size of the sample before and after annealing, high magnifications SEM and TEM images of the sample have been specifically analyzed, as shown in Fig. 5. From the SEM (5a) and TEM (5c) images of the pre-annealed sample, several spheres were randomly selected in the SEM and TEM images. The results reveal that the spheres diameter was about 6 nm, which was also confirmed by TEM observation. Processing continues in this same way on the images after annealing, the results (Fig. 5b, d) show the mean diameter is generally about 8 nm. We deduced that the diameter enlarge of sphere after annealing was because the carbon coating during carbonation process. Precisely because of the ultrafine sphere and existence of the carbon layer, the as-prepared products have excellent stability and good cycling performance when used as anode materials.

The specific and porous C@Cu@SnO_2 spheres have a pretty high specific surface area. Nitrogen adsorption/desorption measurement shows that the C@Cu@SnO_2 composites possess a high Brunauer-Emmett-Teller (BET) specific surface area of *ca.* 305.3 $m^2 g^{-1}$. Fig. 6a displays the nitrogen adsorption and desorption isotherms and Barrett-Joyner-Halenda (BJH) pore size distribution (Fig. 6b). The average pore diameter of the cage-like SnO_2 composites is about 2–5 nm. With such high specific surface area and numerous holes between C@Cu@SnO_2 spheres, there have enough space and gaps around the particles which can hold the inserted Li^+ during charge and discharge process. The electrode will have little volume change and the SnO_2 crystal will keep original structure with the aid of carbon and copper co-encapsulated. Fig. 7 shows the Raman spectrum collected in the range of 1000–2000 cm^{-1} of the C@Cu@SnO_2 composites. Two bands at 1353 and 1586 cm^{-1} are assigned with sp3-hybridized carbon, structural or amorphous carbon (D-band) and the E_{2g} phonon of sp^2 carbon atoms of the carbon (G-band), respectively.

To better understand the electrode reaction processes of the as-prepared C@Cu@SnO_2 electrode, cyclic voltammetric measurements (CV) were carried out with the result shown in Fig. 8a. The CV behavior is generally agreement with that reported in previous papers [22]. The current peak around 0.72 V (versus Li/Li^+), in the following cycles, corresponds to the reductive transformation of SnO_2 to Sn and Li_2O. An apparent cathodic peak located around 0.80 V is observed during the first cycle and no longer appeared in the later cycles, which attributed to the formation of a solid

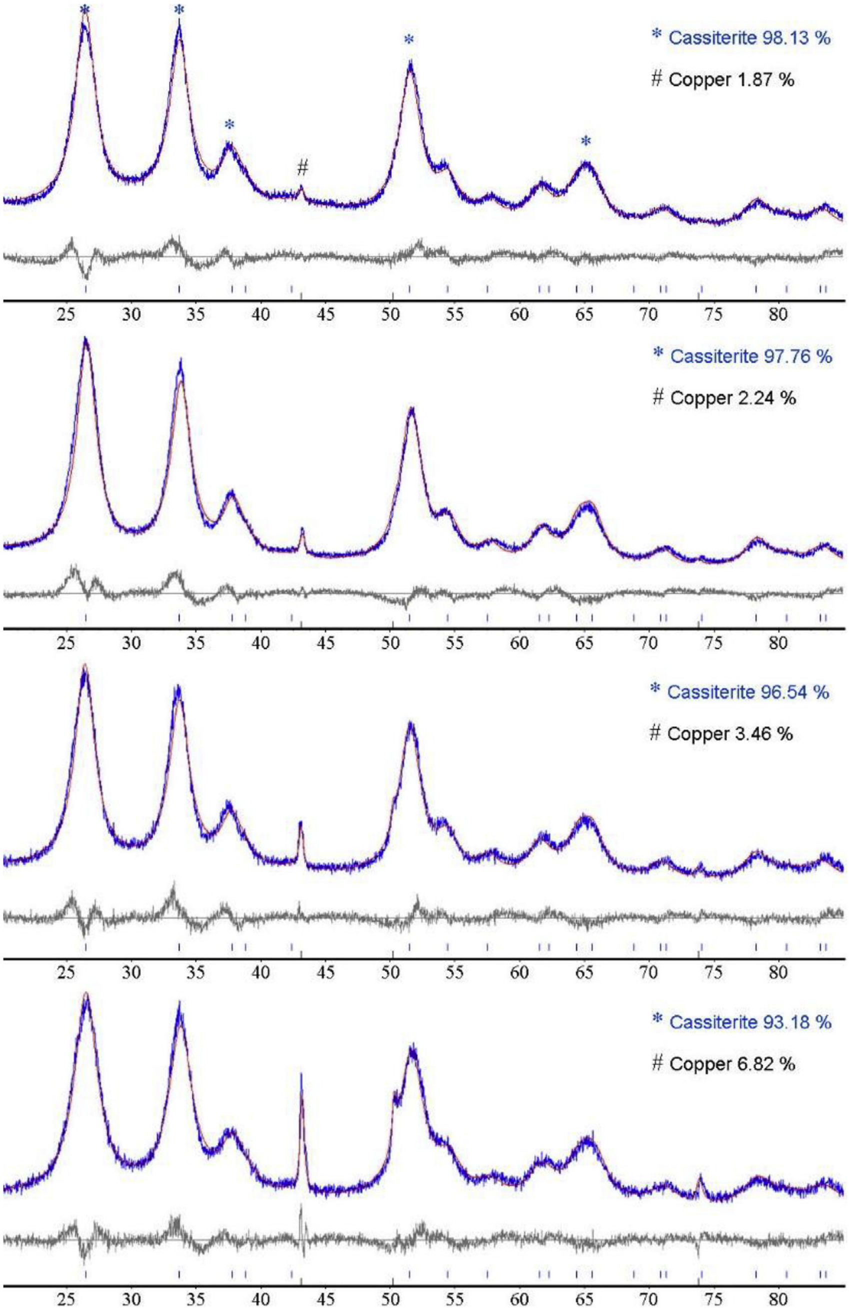

Fig. 2. XRD diffraction patterns analyzed using the TOPAS program of different Cu contents.

electrolyte interface (SEI) layer, which consumes Li ions but can buffer the volume change. The oxidation peak around 0.6 V (versus Li/Li$^+$) are assigned to the alloying process of Li$_x$Sn alloy. Another oxidation peak around 1.30 V (versus Li/Li$^+$) can be assigned to the reactions on the electrode in the electrochemical test. The peak at 0.1 V (versus Li/Li$^+$) can be attributed to formation of Li$_x$Sn alloy and insertion of Li$^+$ into the carbon materials. Fig. 8b shows the typical CV curves of SnO$_2$ without Cu doping.

When evaluated as anode materials for LIBs, the as-synthesized C@Cu@SnO$_2$ composites (20% CuCl$_2$) exhibited good electrochemical performance compared to other C@Cu@SnO$_2$ or SnO$_2$ samples. Fig. 9a shows cycling performance and coulombic efficiency of the C@Cu@SnO$_2$ composites electrode measured in a potential range of 0.01–3 V versus Li$^+$/Li at the current density of 0.2, 0.4 and 0.8 A g^{-1}, respectively. As expected, the composites manifested exceptional capacity retention ability and high-capacity lithium storage properties. It exhibits large initial discharge capacity of about 1449.4 mAh g^{-1} and retains about 670.3 mAh g^{-1} after 50 cycles at the current density of 0.2 A g^{-1}. The coulombic efficiency rises rapidly from 74.4% in the first cycle to 93% in the fifth one and then remains above 99% in the following cycles. When the current density was up to 0.4 and 0.8 A g^{-1}, capacities higher than 632.1 and 565.5 mAh g^{-1} were obtained, respectively, which were even more higher than the theoretical capacity (372 mAh g^{-1}) of graphite. The battery was kept working at the current density of 0.4 A g^{-1} for 200 cycles and the results show that the battery still maintained excellent cycling stability. The reversible capacity is about 452 mAh g^{-1} after 200 charge-discharge cycles as shown in

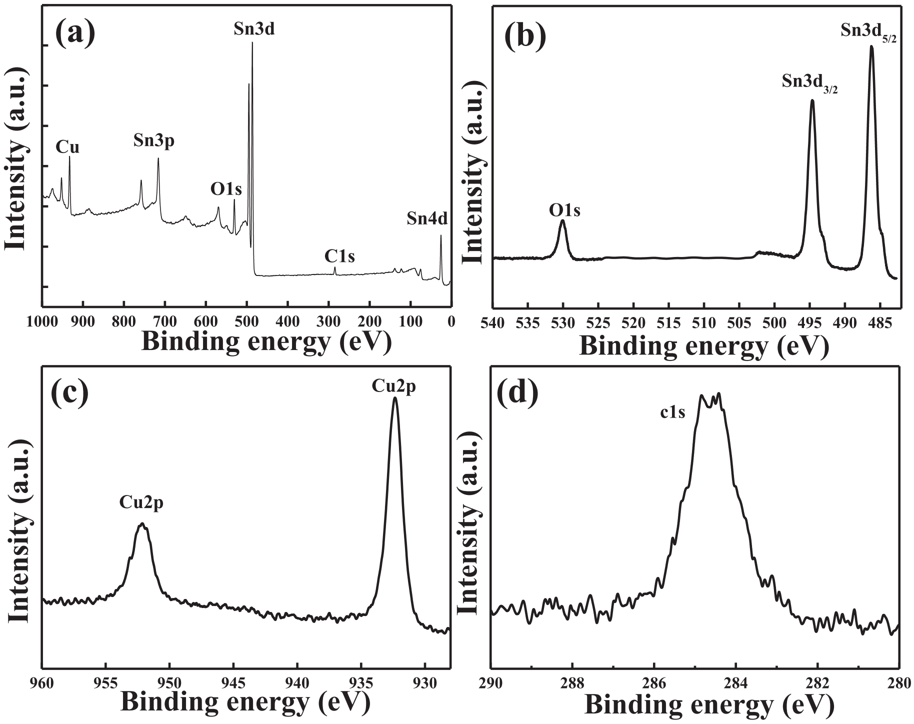

Fig. 3. XPS spectra of C@Cu@SnO$_2$ products: (a) survey spectrum and high-resolution; (b) Sn 3d; (c) Cu 2*p* and (d) C 1s high-resolution spectra.

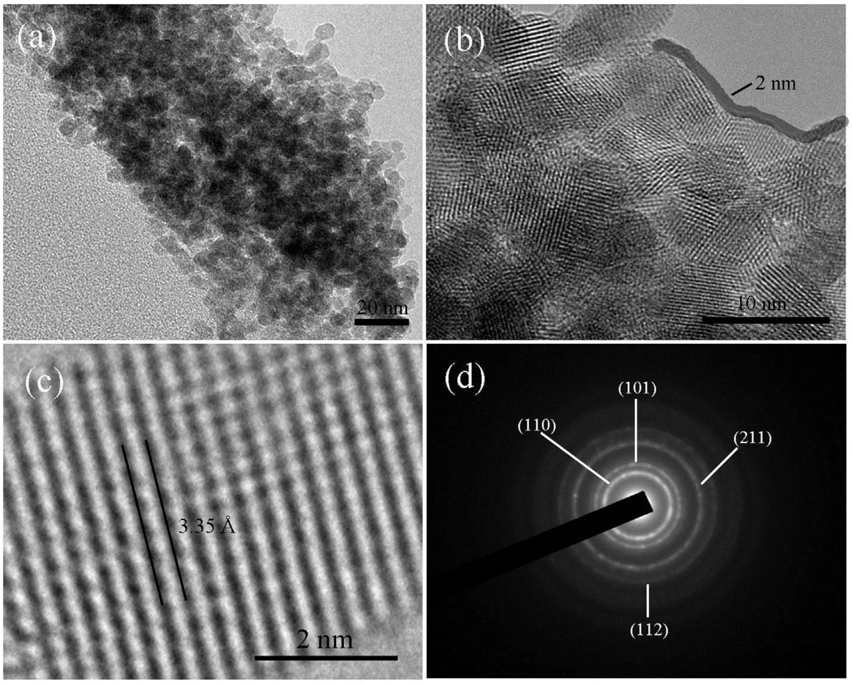

Fig. 4. (a) and (b) Low-magnification TEM image; (c) High-magnification TEM image and (d) SAED pattern of C@Cu@SnO$_2$ products.

insert in Fig. 9a. The good cycling performance indicates that the C@Cu@SnO$_2$ composites may be the alternative anode materials for lithium ion battery in future.

Fig. 9b shows the discharge/charge voltage profiles of the as prepared C@Cu@SnO$_2$ composites for the 1st, 2nd and 5th cycle respectively. The first-discharge and charge capacity were 1449.4 and 1078 mAh·g^{-1}, this can be attributed to the initial irreversible reduction of SnO$_2$ to Sn and the formation of a solid electrolyte interface (SEI) layer. The discharge capacity in the second cycle is 1113 mAh·g^{-1} and 905 mAh·g^{-1} in the fifth cycle. Moreover, the products also exhibited good rate performance because the existence of Cu under all tested current densities. As shown in Fig. 9c, the reversible capacity at the current density of 0.8 A g^{-1} is 568.5 mAh g^{-1} and even at as high as 2 A g^{-1}, it retains high

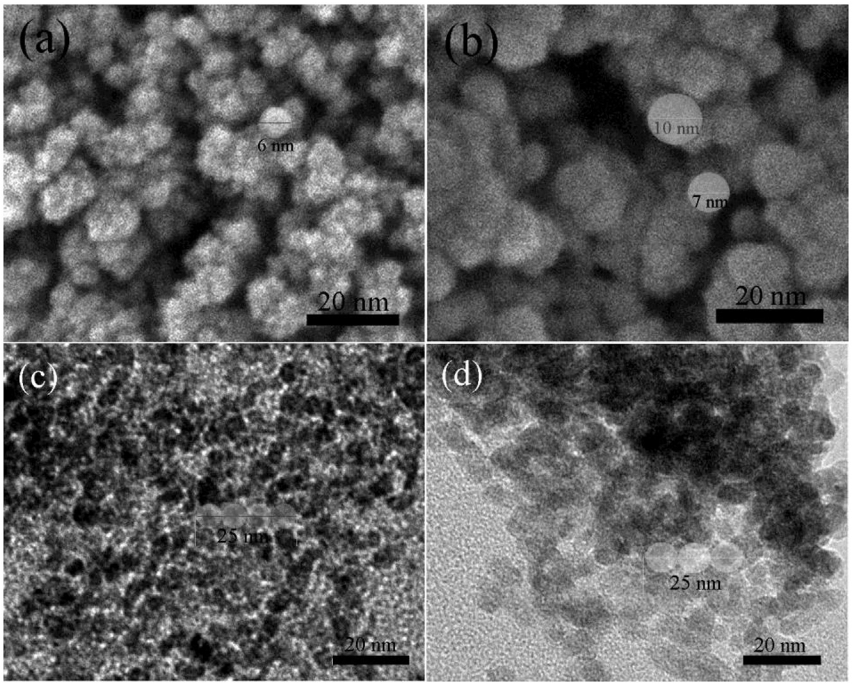

Fig. 5. Enlarged SEM images before (a) and after (b) calcination of the samples; Enlarged TEM images before (c) and after (d) calcination of the $C@Cu@SnO_2$ products.

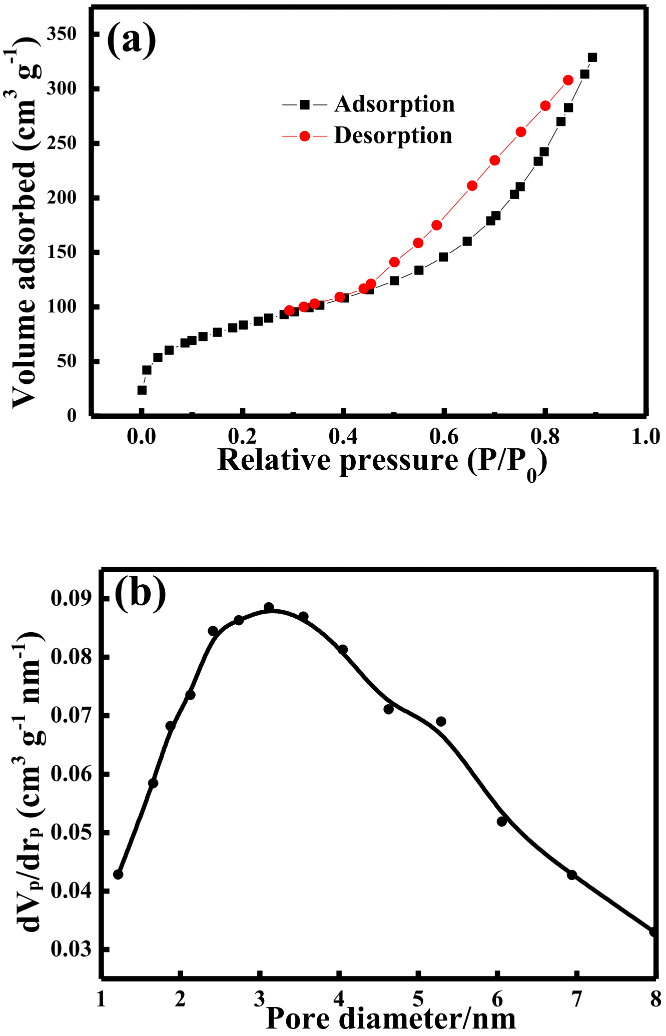

Fig. 6. N_2 adsorption-desorption isotherms at 77 K (a) and pore size distribution curve based on the desorption branch (b) of the $C@Cu@SnO_2$ products.

capacity of 430.6 mAh g^{-1}, which is still higher than the theoretical capacity (372 mAh g^{-1}) of graphite. After the current density returns to 0.2 A g^{-1}, the electrode delivers a capacity of about 740 mAh g^{-1} after 50 cycles. To compare the $C@Cu@SnO_2$ products with different copper content and $C@SnO_2$ (it was synthesized at the same conditions but without $CuCl_2$ in the starting materials), the cycling performance of other products were conducted as shown in Fig. 10. As we can see, the sample with the 1.87% Cu content has the worst properties. The discharge capacity just maintain at 179.5 mA g^{-1} at the current density of 0.4 A g^{-1} after 50 cycles. Along with the increase of the content of copper, the electrochemical properties were improved. The product with 2.24% Cu doped have a higher capacity about 396.7 mA g^{-1} and the product with 3.46% Cu doped have capacity about 526.8 mA g^{-1}. The products with low Cu content all have bad electrochemical cycle stability. When the content of Cu was up to 6.82% (20% $CuCl_2$ as dosage), it retains about 632.1 mAh g^{-1} capacity after 50 cycles at the current density of 0.4 A g^{-1}. The $C@SnO_2$ products also have worse cycling performance at same condition. The improved electrochemical performance of the $C@Cu@SnO_2$ composites illustrated the introduction of copper was an effective way to enhance the conductivity and improve the performance of lithium ion batteries.

To further understand the improved lithium storage performance of the $C@Cu@SnO_2$ electrode at different ratio of Cu, we studied their transport kinetics by electrochemical impedance spectra (EIS) measurements, which were carried out over the frequency range from 100 kHz to 0.1 Hz before cycling [16]. All the Nyquist plots show depressed separate semicircles in high-middle frequency region and a straight line in low frequency region, as shown in Fig. 10, the $C@Cu@SnO_2$ with 20% $CuCl_2$ has the minimum semicircle diameter in the high frequency region among these samples, which is in accordance with the fact and expectation. This is because the existence of Cu indeed reduces the electrical resistance and increase the electrical conductivity effectively.

The improved electrochemical performances of $C@Cu@SnO_2$ composites certainly originated from the following factors. One possible reason is the co-encapsulated of copper and carbon. The carbon and copper shell acts as a buffer layer efficiently alleviating

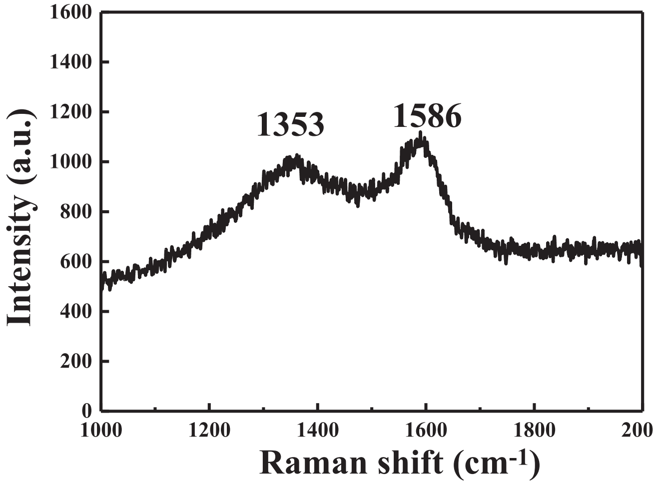

Fig. 7. Raman spectrum of the C@Cu@SnO$_2$ products.

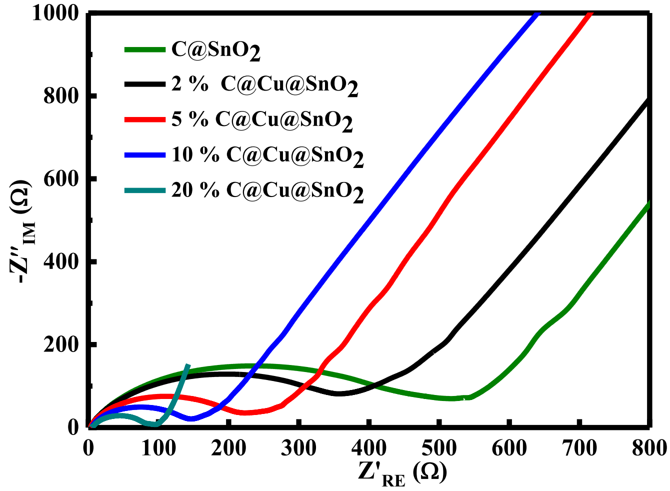

Fig. 10. Electrochemical impedance plots of the different contents of copper of C@Cu@SnO$_2$ and C@SnO$_2$ products.

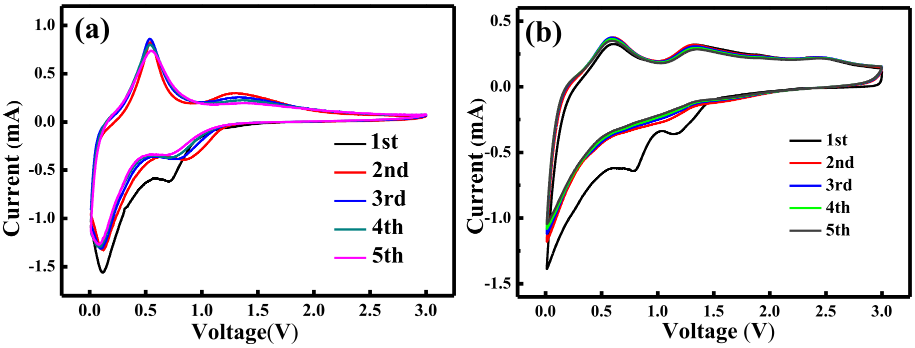

Fig. 8. CV curves of the (a) C@Cu@SnO$_2$ products and (b) C@SnO$_2$.

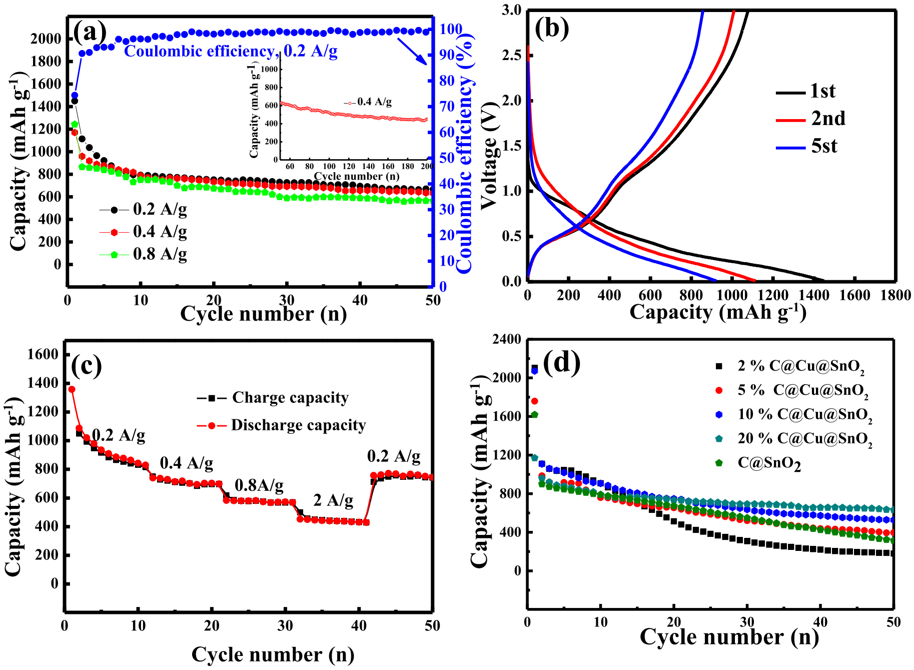

Fig. 9. (a) Cycling performance and coulombic efficiency of the C@Cu@SnO$_2$ products; (b) The discharge-charge voltage profiles (1st, 2nd and 5th); (c) Rate performance and (d) Cycling performance (at a current density of 0.4 A g^{-1}) of different contents of copper of C@Cu@SnO$_2$ and C@SnO$_2$ products.

the volume change during lithium insertion and extraction in the charge/discharge process. Also, the existence of Cu indeed reduces the electrical resistance and increase the electrical conductivity effectively. Another reason is the ultra-small grain of products. Due to the very small size (about 8 nm), the nanoparticles will have bigger specific surface areas. The bigger specific surface areas they have, the more space they will have to contact Li/Li^+ during lithium insertion and extraction. That is helpful for buffering the severe volume change during lithium insertion and extraction. Therefore, copper and carbon co-encapsulated and ultra-small grain could be effective way to improve the cycling performance of tin-dioxide for lithium-ion batteries.

4. Conclusions

In summary, C@Cu@SnO_2 composites constructed with ultrafine grain has been successfully synthesized by a facile hydrothermal method. When used as an anode material for LIBs, the products exhibit excellent cycling performance and high capability. The ultra-fine SnO_2 grain with the copper can increase the conductivity and the ultra-fine SnO_2 grain with the carbon can increase the stability of the active material. The synergistic effect of copper and carbon in the composite materials can effectively improve lithium storage performance. The doping of high conductivity metal to the oxide may be an effective way to improve the performance of lithium ion batteries.

Acknowledgements

We would like to thank the financial support from the National Natural Science Foundation of China (Grant No.: 10974105, 21701095), Natural Science Foundation of Shandong Province, China (Grant No.: ZR2017BEM007), China Postdoctoral Science Foundation (Grant No.: 2017M622131), Program of Science and Technology for Higher Education in Shandong Province, China (Grant No.: J17KA010), the Natural Science Foundation for Outstanding Young Scientist in Shandong Province (Grant No.: JQ201002) and High-end Foreign Experts Recruitment Programs (Grant Nos.: GDW20143500163, GDW20163500110).

References

[1] N.S. Choi, Z.H. Chen, S.A. Freunberger, X.L. Ji, Y.K. Sun, K. Amine, G. Yushin, L.F. Nazar, J. Cho, P.G. Bruce, Challenges facing lithium batteries and electrical double-layer capacitors, Angew. Chem. Int. Ed. 51 (2012) 9994–10024.
[2] F.Y. Cheng, J. Liang, Z.L. Tao, J. Chen, Functional materials for rechargeable batteries, Adv. Mater. 23 (2011) 1695–1715.
[3] M.V. Reddy, G.V. Subba Rao, B.V.R. Chowdari, Metal oxides and oxysalts as anode materials for Li ion batteries, Chem. Rev. 113 (2013) 5364–5457.
[4] K.Z. Cao, L.F. Jiao, H.Q. Liu, Y.C. Liu, Y.J. Wang, Z.P. Guo, H.T. Yuan, 3D hierarchical porous α-Fe_2O_3 nanosheets for high-performance lithium-ion batteries, Adv. Energy Mater. 5 (2015), 1401421.
[5] B. Melot, J.M. Tarascon, Design and preparation of materials for advanced electrochemical storage, Acc. Chem. Res. 46 (2013) 1226–1238.
[6] J.W. Chen, X. Wang, J.X. Wang, P.S. Lee, Sulfidation of NiMn-layered double hydroxides/graphene oxide composites toward supercapacitor electrodes with enhanced performance, Adv. Energy Mater. 6 (2016), 1501745.
[7] Z.X. Chen, M. Zhou, Y.L. Cao, X.P. Ai, H.X. Yang, J. Liu, In situ generation of few-layer graphene coatings on SnO_2-SiC core-shell nanoparticles for high-performance lithium-ion storage, Adv. Energy Mater. 2 (2012) 95–102.
[8] J.S. Chen, X.W. Lou, SnO_2-based nanomaterials: synthesis and application in lithium-ion batteries, Small 9 (2013) 1877–1893.
[9] M.V. Reddy, G.V.S. Rao, B.V.R. Chowdari, Metal oxides and oxysalts as anode materials for Li ion batteries, Chem. Rev. 113 (2013) 5364–5457.
[10] (a) G.C. Xi, J.H. Ye, Ultrathin SnO_2 nanorods: template- and surfactant-free solution phase synthesis, growth mechanism, optical, gas-sensing, and surface adsorption properties, Inorg. Chem. 49 (2010) 2302–2309;
(b) X.X. Xu, J. Zhuang, X. Wang, SnO_2 quantum dots and quantum wires: controllable synthesis, self-assembled 2D architectures, and gas-sensing properties, J. Am. Chem. Soc. 130 (2008) 12527–12535;
(c) B. Liu, M.H. Cao, X.Y. Zhao, Y. Tian, W.C. Hu, Facile synthesis of ultrafine carbon-coated SnO_2 nanoparticles for high-performance reversible lithium storage, J. Power Sources 243 (2013) 54–59.
[11] L.F. Shen, Q. Che, H.S. Li, X.G. Zhang, Mesoporous $NiCo_2O_4$ nanowire arrays grown on carbon textiles as binder-free flexible electrodes for energy storage, Adv. Funct. Mater. 24 (2014) 2630–2637.
[12] X.Y. Zhao, B. Liu, C.W. Hu, M.H. Cao, In situ growth of hierarchical SnO2 nanosheet arrays on 3D macroporous substrates as high-performance electrodes, Chem. Eur. J. 20 (2014) 467–473.
[13] (a) Z.Y. Wang, D.Y. Luan, F.Y.C. Boey, X.W. Lou, Fast formation of SnO_2 nanoboxes with enhanced lithium, storage capability, J. Am. Chem. Soc. 133 (2011) 4738–4741;
(b) S.J. Ding, J.S. Chen, G.G. Qi, X.N. Duan, Z.Y. Wang, E.P. Giannelis, L.A. Archer, X.W. Lou, Formation of SnO_2 hollow nanospheres inside mesoporous silica nanoreactors, J. Am. Chem. Soc. 133 (2011) 21–23;
(c) T. Zhang, H. Liang, C.D. Xie, H.L. Qiu, Z.B. Fang, L. Wei, H.J. Yue, G. Chen, Y.J. Wei, C.Z. Wang, D. Zhao, Morphology-controllable synthesis of spinel zinc manganate with highly reversible capability for lithium ion battery, Chem. Eng. J. 326 (2017) 820–830;
(d) L. Zhang, H.B. Wu, B. Liu, X.W. Lou, Formation of porous SnO_2 microboxes via selective leaching for highly reversible lithium storage, Energy Environ. Sci. 7 (2014) 1013–1017.
[14] L. Xia, S.Q. Wang, G.X. Liu, L.X. Ding, D.D. Li, H.H. Wang, S.Z. Qiao, Flexible SnO_2/N-doped carbon nanofiber films as integrated electrodes for lithium-ion batteries with superior rate capacity and long cycle life, Small 12 (2016) 853–859.
[15] (a) G. kucinskis, G. Bajars, J. Kleperis, Graphene in lithium ion battery cathode materials: a review, J. Power Sources 240 (2013) 66–79;
(b) X.S. Zhou, L.J. Wan, Y.G. Guo, Binding SnO_2 nanocrystals in nitrogen-doped graphene sheets as anode materials for lithium-ion batteries, Adv. Mater. 25 (2013) 2152–2157;
(c) N. Li, M.H. Cao, C.W. Hu, Review on the latest design of graphene-based inorganic materials, Nanoscale 4 (2012) 6205–6218.
[16] H.K. Wang, A.L. Rogach, Hierarchical SnO_2 nanostructures: recent advances in design, synthesis, and application, Chem. Mater. 26 (2014) 123–133.
[17] M. Park, X.C. Zhang, M. Chung, G.B. Less, A.M. Sastry, A review of conduction phenomena in Li-ion batteries, J. Power Sources 195 (2010) 7904–7929.
[18] L. Lu, Y.F. Shen, X.H. Chen, L.H. Qian, K. Lu, Ultrahigh strength and high electrical conductivity in copper, Science 304 (2004) 422–426.
[19] J.W. Deng, C.L. Yan, L.C. Yang, S. Baunack, S. Oswald, H. Wendrock, Y.F. Mei, O.G. Schmidt, Sandwich-stacked SnO_2/Cu hybrid nanosheets as multichannel anodes for lithium ion batteries, ACS Nano 7 (2013) 6948–6954.
[20] (a) S.Y. Zheng, P. Han, Z. Han, P. Li, H.J. Zhang, J.H. Yang, Nano-copper-assisted immobilization of sulfur in high-surface-area mesoporous carbon cathodes for room temperature Na-S batteries, Adv. Energy Mater. 4 (2014) 1400226;
(b) W. Xu, N.L. Ganfield, D.Y. Wang, J. Xiao, Z.M. Nie, J.G. Zhang, A three-dimensional macroporous Cu/SnO2 composite anode sheet prepared via a novel method, J. Power Sources 195 (2010) 7403–7408;
(c) S.C. Zhang, Y.L. Xing, T. Jiang, Z.J. Du, F. Li, L. He, W.B. Liu, A three-dimensional tin-coated nanoporous copper for lithium-ion battery anodes, J. Power Sources 196 (2011) 6915–6919.
[21] X. Xu, S. Chen, C.H. Xiao, K. Xi, C.W. Guo, S.W. Guo, S.J. Ding, D.M. Yu, R. Vasant Kumar, Rational Design of $NiCoO_2$@SnO_2 heterostructure attached on amorphous carbon nanotubes with improved lithium storage properties, ACS Appl. Mater. Interfaces 8 (2016) 6004–6010.
[22] X.S. Zhou, L. Yu, X.W. Lou, Formation of uniform N-doped carbon-coated SnO_2 submicroboxes with enhanced lithium storage properties, Adv. Energy Mater. 6 (2016), 1600451/1-6.
[23] V. Stengl, T.M. Grygar, J. Henych, M. Kormunda, Hydrogen peroxide route to Sn-doped titania photocatalysts, Chem. Cent. J. 6 (2012) 113.
[24] M. Kwoka, L. Ottaviano, M. Passacantando, S. Santucci, G. Czempik, J. Szuber, XPS study of the surface chemistry of L-CVD SnO_2 thin films after oxidation, Thin Solid Films 490 (2005) 36–42.
[25] B. Liu, X.Y. Zhao, Y. Tian, D. Zhao, C.W. Hu, M.H. Cao, A simple reduction process to synthesize MoO_2/C composites with cage-like structure for high-performance lithium-ion batteries, Phys. Chem. Chem. Phys. 15 (2013) 8831–8837.